Energy Transfer Kinetics and Low Energy Vibrational Structure of the Three Lowest Energy Q_y-States of the Fenna−Matthews−Olson Antenna Complex

S. Matsuzaki, V. Zazubovich, M. Rätsep,† J. M. Hayes, and G. J. Small*

Ames Laboratory-USDOE and Department of Chemistry, Iowa State University, Ames, Iowa 50011

Received: May 18, 2000; In Final Form: August 1, 2000

Burn wavelength (λ_B)-dependent nonphotochemical hole spectra are reported for the lowest energy Q_y-absorption band of the Fenna−Matthews−Olson (FMO) trimer complex from *Prosthecochloris aestuarii*. This band at 825 nm is contributed to by three states that stem from the lowest energy state of the subunit of the trimer. The spectra reveal unusually rich and quite sharp low energy satellite structure that consists of holes at 18, 24, 36, 48, 72, 120, and 165 cm^{-1} as measured relative to the resonant hole at λ_B. The possibility that some of these holes are due to correlated downward energy transfer from the two higher energy states that contribute to the 825 nm band could be rejected. Thus, the FMO complex is yet another example of a photosynthetic complex for which structural heterogeneity results in distributions for the values of the energy gaps between Q_y-states. The results of theoretical simulations of the hole spectra are consistent with the above holes being due to intermolecular phonons and low energy intramolecular vibrations of the bacteriochlorophyll *a* (BChl *a*) molecule. The 36 cm^{-1} and higher energy modes are most likely due to the intramolecular BChl *a* modes. The simulations lead to the determination of the Huang−Rhys (S) factor for all modes. They range between 0.05 and 0.25 in value. The temperature dependencies of the spectral dynamics for the three contributing states are similar to those reported for the FMO complex from *Chlorobium tepidum* (Rätsep et al., *J. Phys. Chem. B* **2000**, *103*, 5736). The contribution to the dynamics from pure dephasing/spectral diffusion due to the glasslike two-level systems of the protein is identical for all three states. The lifetimes of the highest and intermediate energy Q_y-states due to downward energy transfer are 26 and 99 ps, respectively, at liquid helium temperatures.

1. Introduction

The Fenna−Matthews−Olson (FMO) bacteriochlorophyll *a* (BChl *a*) antenna complex of the green sulfur bacterium *Prosthecochloris aestuarii* was the first photosynthetic complex whose structure was determined by X-ray diffraction.[1] The structure led to many studies of its $Q_y(S_1)$-electronic structure and excitation energy transfer (EET) dynamics (for reviews see refs 2 and 3). The complex is a C_3 trimer of subunits, each containing seven symmetry inequivalent BChl *a* molecules. Nearest neighbor Mg···Mg distances within the subunit are ≈ 11−14 Å with the largest pairwise excitonic couplings in the ≈ 50−200 cm^{-1} range (calculated using point monopoles with a dielectric constant, ϵ, of 1 [4]). The largest coupling between BChl *a* molecules belonging to different subunits is ≈ 15 cm^{-1}. Recently, the X-ray structure of the FMO complex from *Chlorobium tepidum* was determined.[5] The relative orientations of the BChl *a* molecules and the distances between them are very similar to those of *P. aestuarii*, although there are some potentially significant differences in H-bonding and BChl *a*-residue distances that may contribute to the differences between the 4.2 K Q_y-absorption spectra of *P. aestuarii* and *Cb. tepidum* seen in Figure 1.

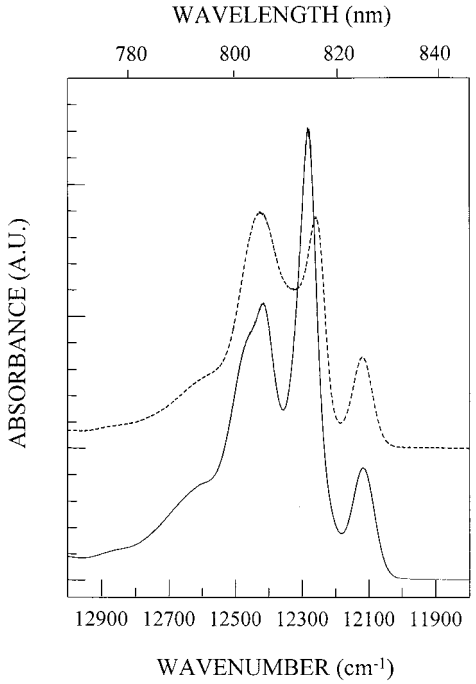

Figure 1. The 4.2 K Q_y-absorption spectrum of the FMO complex from *P. aestuarii* (solid curve) and *Cb. tepidum* (dashed curve).

Pearlstein and co-workers were the first to perform excitonic calculations on the FMO complex of *P. aestuarii*. In the end, Pearlstein concluded that it is necessary to include the full trimer, rather than just the subunit, to best explain the low-temperature absorption and CD spectra.[4] Consideration of the trimer was stimulated by the 4.2 K hole burning results of Johnson and

* To whom correspondence should be addressed. E-mail: *gsmall@ameslab.gov*.

† Current address: Institute of Physics, 142 Riia St., Tartu 51014, Estonia.

10.1021/jp0018495 CCC: $19.00
Published on Web 09/08/2000

Small,[6] which showed that the 825 nm absorption band (see Figure 1) is contributed to by at least two states. van Mourik et al.[7] reached the same conclusion based on polarized triplet−singlet difference spectra. Concerning the states of the subunit, Pearlstein found that they are mini-excitons with excitation primarily on 2−3 BChl *a* molecules. The mini-exciton picture also emerged from the calculations of Gülen[8] and Louwe et al.[9] There is general agreement that the 825 nm absorption band is due to three trimer states that stem from the lowest energy Q_y-state of the subunit that is mainly localized on a single BChl *a* molecule. This molecule is most likely BChl 3[9] or 6,[8] according to the numbering scheme of ref 1. For perfect C_3 symmetry, there is a doubly degenerate E state and a nondegenerate A state, which are polarized perpendicular and parallel to the C_3-axis, respectively. Energy disorder due to structural heterogeneity results in removal of the degeneracy of the E state and mixing of the A and E states. On the basis of results of Gülen[8] and Louwe et al.,[9] it is most likely that the A state is weakly absorbing relative to the E state in the absence of energy disorder. However, which of these two states lies lowest in energy is an unsettled question.

Further evidence for the 825 nm band being contributed to by three states came from the low-temperature accumulated photon echo experiments of Louwe and Aartsma[10] on the FMO complex of *P. aestuarii* and the nonphotochemical hole burning experiments of Rätsep et al.[11] on the FMO complex of *Cb. tepidum*. Both works showed that the lifetimes of states excited at the high energy side and maximum of the 825 nm band are significantly shorter than that of the state excited at the low energy side which is 2 ns, about the value expected for the lifetime of an isolated BChl *a* molecule. The hole burning data led to lifetime values of 117 and 37 ps for λ_B (burn wavelength) equal to 825 and 823 nm, respectively, which are similar to those reported by Louwe and Aartsma. Both groups concluded that these two lifetimes are determined by downward excitation energy transfer (EET). On the basis of the fitting of the 825 nm absorption band of *Cb. tepidum*, Rätsep et al.[11] suggested that it is contributed to by the absorption bands of three states located near 823, 825, and 827 nm, with each band carrying a static inhomogeneous broadening of about 50 cm^{-1} and the same intensity. This suggests that one may be in the strong energy disorder limit. However, the results of van Mourik et al.[7] argue against this limit.

Presented here are nonphotochemical hole burning (NPHB) data and spectra for the FMO complex of *P. aestuarii*. There were two main objectives of the experiments. The first was to elucidate the excitation energy transfer (EET) and spectral dynamics of the three trimer states that contribute to the 825 nm band and compare them with those of *Cb. tepidum*. The results show that the kinetics for downward EET from the two higher energy states are similar in the two species as is the temperature dependence (1.8−10 K) of the spectral dynamics due to the two-level systems (TLS) of the protein. The second objective was to obtain more[12] detailed spectra that report on the unusual and rich *low* energy satellite hole structure observed when the burn wavelength (λ_B) is tuned from the low to high energy side of the 825 nm band. The energies of the satellite holes, as measured relative to the resonant zero-phonon hole at λ_B, are in the range 18 to ∼120 cm^{-1}. The results lead to two possible interpretations for the satellite structure: that it is due to pseudo-phonon sideband holes, and/or that it is due to correlated downward EET from higher to lower energy states. It is emphasized that both interpretations are relevant to the interpretation of the EET kinetics. It is concluded that the first interpretation is correct and that the satellite structure is due to both intermolecular phonons and very low-frequency intramolecular modes of BChl *a*.

2. Materials and Methods

Samples of the isolated FMO complex from *P. aestuarii* were kindly provided by Professor T. Aartsma at Leiden University. The green sulfur bacterium was grown in a mixed culture as described in.[13] The protein was isolated and purified as described by Francke and Amesz.[14] Complexes were dissolved in 50 mM HCl-Tris buffer at pH 8.3. Glycerol was added (70% v/v) to ensure good glass formation. Samples were contained in gelatin or plastic capsules with an optical path length of 5 and 8 mm, respectively. The optical density of the sample at 825 nm was adjusted to ∼0.3 at 4 K. A Janis 20 DT liquid helium cryostat was used for low-temperature measurements. Temperatures were stabilized with a Lakeshore Cryotronics Model 330 temperature controller and measured with a silicon diode (accuracy ± 0.1 K).

The laser used for hole burning was a Coherent CR899−29 Autoscan Ti:Sapphire laser pumped by a 15 W Coherent Innova 200 Ar-ion laser. The laser intensity was stabilized using an LS 100 power stabilizer (Cambridge Research and Instrumentation.) The burn intensities and times used are given in the Figure captions.

The hole spectra were obtained with the thick etalon of the above Ti:sapphire laser removed which led to a line width of 0.07 cm^{-1}. The spectra were recorded with a Bruker IFS 120 HR Fourier transform (FT) spectrometer operated at a resolution of 1 cm^{-1}. Hole spectra are the difference between the post-burn and pre-burn spectra. Most of the spectra reported are the average of 200 scans with an acquisition time of 8 min. The intensity of the white light from the spectrometer at the sample was ∼2 mW/cm^2. A Glan-Thompson polarizer was used in the polarized hole burning experiments and placed before the sample, in-line with the spectrometer's white light beam. The vertically polarized laser beam was perpendicular to the optical axis. Post-burn spectra were recorded with horizontal polarization first and vertical polarization second. (Preburn absorption spectra were recorded with vertical and horizontal polarization of the probe beam in order to account for the possibility that the probe beam of the FT spectrometer is slightly polarized.) This order was chosen because of the spontaneous hole filling (SPHF), whose kinetics are dispersive; easier to burn sites are easier to fill.[15] It ensures that any polarization effects observed for the low energy satellite hole structure are real. This structure was observed to be uniformly and preferentially polarized parallel to the laser polarization.

For measurement of the dependence of the widths of zero-phonon holes on temperature, the above Ti:sapphire laser was used with an actively stabilized line width < 20 MHz. Spectra were recorded in the fluorescence excitation mode. Fluorescence was detected and processed by a GaAs photomultiplier tube (Hamamatsu) and photon counter (SR-400, Stanford Research Instruments). Rejection of scattered laser light was accomplished with two long wavelength-pass filters (RG 850, Coherent-Ealing) and a broad band interference filter (P60−940, Coherent-Ealing). This combination allowed for fluorescence detection between ∼910 and 930 nm. Laser intensities used for hole burning were in the range 20−400 $\mu W/cm^2$, depending on the burn wavelength. Hole depths were typically ∼10%. For hole reading, the laser was attenuated by a factor of 10−100 in order to avoid hole burning during reading.

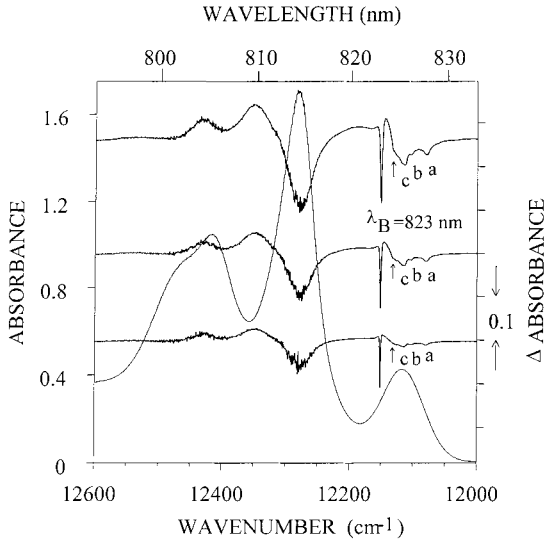

Figure 2. Hole burned spectra of the FMO complex from *P. aestuarii* obtained with burn wavelength (λ_B) = 823.0 nm at 4.2 K. For convenience, the absorption spectrum is also shown. From top to bottom, the burn intensity and burn time used were 50 mW/cm^2, 30 s; 100 mW/cm^2, 75 s; and 100 mW/cm^2, 375 s. The deepest and sharpest hole in each spectrum is the resonant zero-phonon hole at λ_B = 823.0 nm. The solid arrows locate the 18 cm^{-1} pseudo-phonon sideband hole (PSBH). The satellite holes a, b, and c correspond to those indicated in Figures 4 and 5. The broad and higher energy holes are the result of the structural changes that accompany hole burning in the 825 nm absorption band. The structural changes alter the energies of the states that contribute to the higher energy absorption band, see text.

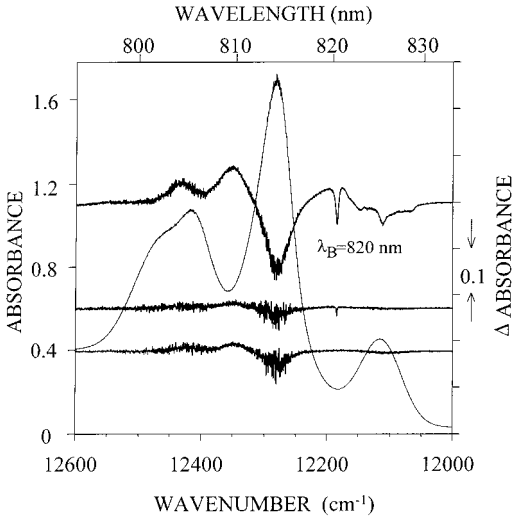

Figure 3. Spectra of the FMO complex from *P. aestuarii* related to the white light hole burning effect, cf. text for discussion. For convenience, the absorption spectrum is also shown. The excessive noise in the spectra near 815 nm is due to the high absorbance. T = 4.2 K.

3. Results and Discussion

Some General Features of the Hole Spectra. Persistent NPHB spectra for the FMO complex of *P. aestuarii* were obtained with burn wavelengths (λ_B) between 805.0 and 829.3 nm. For each λ_B-value spectra were recorded with several burn fluences. Figure 2 shows hole spectra obtained with λ_B = 823 nm, which is at the high energy side of the 825 nm band. For ease of discussion, the absorption spectrum is also shown. The sharpest and deepest zero-phonon hole (ZPH) is coincident with λ_B, referred to hereafter as the resonant hole. The satellite holes a, b, and c are part of the low energy satellite hole structure referred to in the Introduction. The feature indicated by the arrow is a pseudo-phonon sideband hole (PSBH) associated with the resonant hole, vide infra. It is displaced from the resonant hole by 18 cm^{-1}. The broad satellite features at wavelengths shorter than 823 nm are very similar to those observed by Johnson and Small and, recently, by Franken et al.[12] The positive absorption to the left of the broad and relatively intense hole at ~814 nm is its blue-shifted anti-hole (positive absorption) that is a signature for NPHB of S_1 $\pi\pi^*$ states.[16,17] This anti-hole is interfered with by the holes associated with 805 and 800 nm absorption bands. Johnson and Small favored the interpretation that has the high energy satellite holes being due to their associated Q_y-states being excitonically correlated with the state(s) directly burned at λ_B. It is possible, however, that they are due, at least in part, to structural changes produced by NPHB of the state at λ_B that are not localized near the BChl molecules that contribute to it. That is, the structural change is spatially extended. This mechanism, however, is unimportant for the bacterial reaction center of *Rhodopseudomonas viridis*[18] and the LHC II and CP29 antenna complexes of photosystem II.[19,20]

Franken et al.[12] suggested that the afore-mentioned high energy satellite holes might be mainly due to white light hole burning,[21] the white light being that of the Fourier transform spectrometer used by Johnson and Small[6] to record the pre- and post-burn spectra. The results in Figure 3 show that this is not the case. The lowest Δ-absorbance spectrum is the difference between two consecutively recorded absorption spectra, each of which are the average of 100 scans taken at 1.0 cm^{-1} resolution. The acquisition time was 4 min. and the intensity of the white light at the sample was ~2 mW/cm^2. (The conditions used to record the other hole spectra reported here are the average of 200 scans.) The fractional depth of the hole at ~815 nm is only 0.02. Thus, the white light hole burning effect is weak. The sample was then irradiated at λ_B = 820 nm with a laser intensity of 10 mW/cm^2 for 30 s, and the absorption spectrum was recorded. The difference between it and the preceding spectrum is the middle spectrum in Figure 3. The ZPH at λ_B is just discernible, and the fractional absorbance change of the weak hole at ≈ 815 nm is reduced to 0.01. The top hole spectrum was obtained following additional laser irradiation at 820 nm with an intensity of 100 mW/cm^2 for 375 s. The high energy satellite holes near 815, 805, and 800 nm are now much more pronounced. Thus, it may be concluded that the high energy satellite holes of the top spectrum are mainly due to the structural changes that accompany hole burning at λ_B, in agreement with the conclusion reached by Johnson and Small.[6] This is also the case for the hole spectra shown in Figure 2 (see caption for burn intensities and burn times).

Low Energy Satellite Hole Structure. Figure 4 shows hole spectra obtained with nine λ_B-values between 818.0 and 829.3 nm. Except for the λ_B = 824.7 and 829.3 nm spectra, the laser intensity and burn time used were 100 mW/cm^2 and 375 s, respectively (see the caption of Figure 2). For ease of discussion, the absorption spectrum is also shown (dashed curve). The deepest ZPH in each spectrum at λ_B is the resonant hole. The fractional hole depths and widths of the resonant holes are given in the figure caption. The widths of the resonant holes are determined by saturation broadening and the read resolution of 1 cm^{-1}.

Considered first is the bottom spectrum, λ_B = 829.3 nm. At this wavelength, excitation should be at the red edge of the absorption due to the lowest energy state that contributes to the 825 nm band. The dashed and solid arrows locate satellite holes displaced from the resonant hole by +18 and −18 cm^{-1},

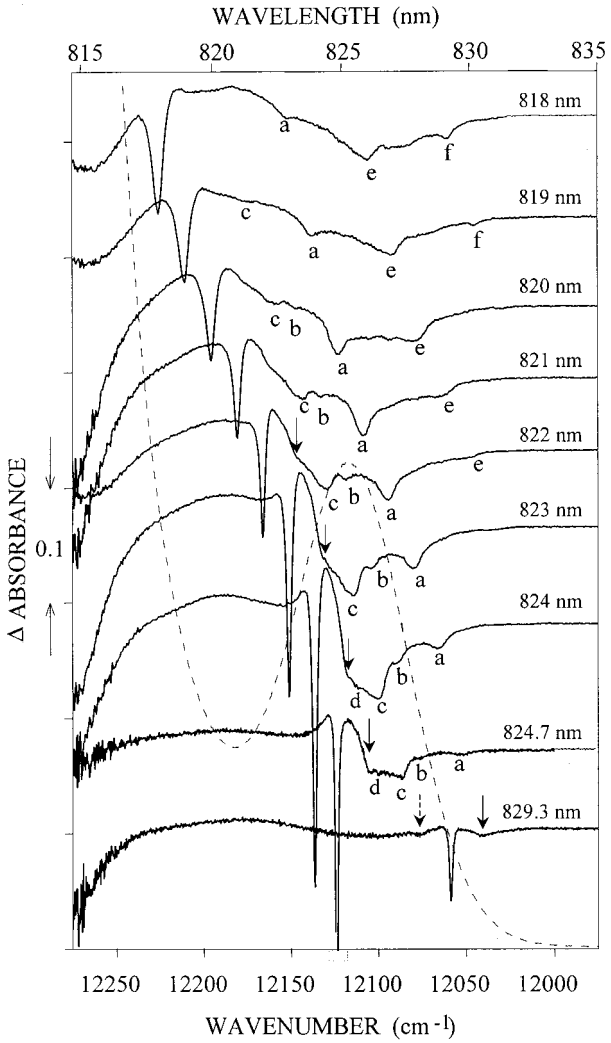

Figure 4. The dependence of the 4.2 K hole burned spectrum of the FMO complex from *P. aestuarii* on burn wavelength (818.0−829.3 nm). The deepest hole in each spectrum is the resonant zero-phonon hole located at λ_B. The burn intensities and times used to obtain the $\lambda_B = 818-824$ nm spectra were 100 mW/cm^2 and 375 s. The intensity and time for the $\lambda_B = 824.7$ and 829.3 nm were 125 mW/cm^2/180 s and 250 mW/cm^2/660 s, respectively. The solid arrows locate the 18 cm^{-1} pseudo-PSBH; the dashed arrow in the $\lambda_B = 829.3$ nm locates the real-PSBH due to the 18 cm^{-1} phonon. The energies of holes a−f as measured relative to λ_B are given in Table 1. The dashed curve is the absorption spectrum. The fractional hole depths of the resonant hole are, from top to bottom, 0.34, 0.34, 0.42, 0.49, 0.43, 0.68, 0.75, 0.61, and 0.75, respectively. The corresponding holewidths are 6.8, 6.7, 4.2, 3.0, 3.0, 2.6, 1.6, and 2.0 cm^{-1}.

respectively. That the satellite holes are symmetrically disposed relative to the resonant hole establishes that they are real- and pseudo-phonon holes (PSBH), respectively. The saturated fractional hole depth of the resonant hole is 0.75. To a good approximation, this depth is given by exp(−S),[22] the Franck−Condon factor for the zero-phonon line. The variable *S* is the Huang−Rhys factor. The result is $S = 0.3$ (weak coupling), in agreement with the value reported in ref 6. The absence of any observable real-PSBH in the $\lambda_B = 829.3$ nm spectrum that lie higher in energy than the 18 cm^{-1} real-PSBH means that the Franck−Condon factors of their associated phonons are smaller than that of the phonon(s) associated with the 18 cm^{-1} hole. We return to this later. We note that the 18 cm^{-1} pseudo-PSBH is also indicated in the $\lambda_B = 824.7$, 824.0, 823.0, and 822.0 nm hole spectra by a solid arrow. As expected, it tracks the resonant hole at λ_B in a linear fashion (± 1 cm^{-1} uncertainty).

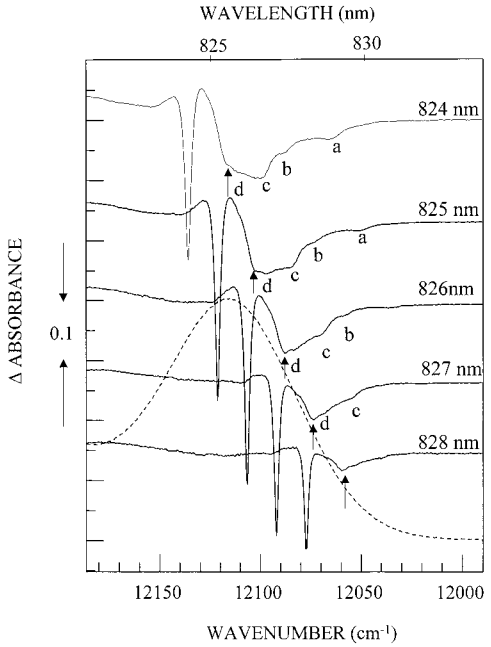

Figure 5. Low energy satellite hole structures obtained with $\lambda_B = 824.0-828.0$ nm, $T = 4.2$ K. Burn intensity and time were ~ 200 mW/cm^2 and up to 1500 s. The deepest hole in each spectrum is the resonant zero-phonon coincident with the burn wavelength (λ_B). The spectra more clearly establish the existence of hole d. The dashed curve is the 825 nm absorption band.

TABLE 1. Spectral Data of the Low Energy Satellite Holes, *P. Aestuarii*

hole	Δ(cm^{-1})[b]	Δ*A*[c]	width (cm^{-1})[d]
pseudo-PSBH[a]	18	0.08	10
a	72	0.023	10
b	48	0.008	5
c	36	0.02	9
d	24	0.004	5
e	120	0.014	9
f	165	0.015	10

[a] PSBH = phonon sideband hole. [b] Displacement measured relative to resonant zero-phonon hole at burn wavelength. [c] Δ-absorbance value for hole when located near the maximum of the 825 nm band. [d] Full width at half-maximum, ± 2 cm^{-1}.

Considered next is the low energy satellite hole structure in Figure 4 that consists of holes a−f. To the best of our knowledge, such rich structure has not been observed in the hole spectra of other photosynthetic complexes. (The 18 cm^{-1} pseudo-PSBH and holes a−d were also observed for *Cb. tepidum*, results not shown.) The hole spectra of Figure 5 show, more clearly, the existence of hole d. With Δ_i defined as the displacement between the resonant hole at λ_B and satellite hole *i*, Δ_i = 72, 48, 36, 24, 120 and 165 cm^{-1} for *i* = a−f, respectively, as given in Table 1. The satellite holes track the resonant hole (λ_B), to within ± 1 cm^{-1}. An analysis of the $\lambda_B = 824-820$ nm spectra in Figure 5 revealed that the 18 cm^{-1} pseudo-PSBH and holes a−d attain their maximum intensity (Δ-absorbance value) when they are located near the maximum of the 825 nm band. From hole burning theory,[22] this is consistent with the satellite hole structure being due to pseudo-PSBH, vide infra. (In what follows, our use of the term phonon is meant to encompass low-frequency intermolecular modes and very low-frequency intramolecular modes of BChl *a*.[23]) The intensities of holes a−d relative to the 18 cm^{-1} pseudo-PSBH, as estimated on the basis of spectra where holes a−d and the 18 cm^{-1} pseudo-PSBH are near the maximum of the 825 nm

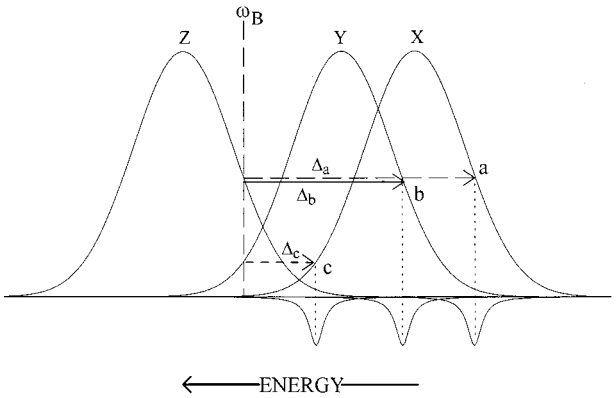

Figure 6. Schematic of correlated downward energy transfer that results in satellite holes a, b, and c displaced from the burn frequency ω_B by Δ_a, Δ_b, and Δ_c. Z, Y, and X denote the three Q_y-states that contribute to the 825 nm band.

absorption band, are given in Table 1. The 18 cm^{-1} hole and hole d ($\Delta_d = 24$ cm^{-1}) are considered to be due to intermolecular modes because their energies are too low to be assigned to intramolecular modes of BChl *a*.[23]

The interpretation that has holes a−f due to pseudo-PSBH will be referred to as interpretation A. There is, however, an alternative interpretation (B). It has holes a, b, and c due to correlated, downward EET from the two higher states that contribute to the 825 nm absorption band. (Hole d would be assigned as a 24 cm^{-1} pseudo-PSBH.) The basic idea behind interpretation B is depicted in Figure 6 where Z,Y,X label the three inhomogeneously broadened absorption bands that contribute to the 825 nm band. Not shown in the figure is the resonant hole at ω_B. Excitation at ω_B selects two isochromats, one at the low energy side of the Z band and the other at the high side of the Y band. Isochromat Z can transfer energy to state Y (solid arrow), whereupon hole burning occurs to produce the center satellite hole displaced from ω_B by Δ_b. It can also transfer to state X (long dashed arrow), whereupon hole burning occurs to produce the right-most hole displaced from ω_B by Δ_a. We note that if the site excitation distribution functions (SDF) of the three states are correlated, as defined below, the Z→Y→X EET pathway also leads to a hole at Δ_a. Isochromat Y, selected by ω_B, can transfer energy to state X, whereupon hole burning ensues to produce the left-most hole displaced from ω_B by Δ_c. If the SDF of the three states are correlated, the satellite holes should track ω_B, i.e., Δ_a, Δ_b, Δ_c should be independent of the ω_B-value, vide infra.

We now define what is meant by correlated. Consider states Z and X. Let $\omega_Z = \bar{\omega}_Z + z$ and $\omega_X = \bar{\omega}_X + x$ be frequencies associated with their SDF. ($\bar{\omega}_Z$ and $\bar{\omega}_X$ are the peak frequencies of the SDF which can be reasonably taken to be Gaussians.) For linear correlation, $x = \alpha y$ where α is a constant. Thus, excitation at $z = \omega_B$ should result in a low energy satellite hole displaced from ω_B by $\Delta_a = (\bar{\omega}_Z - \bar{\omega}_X) + (1 - \alpha)z$. Perfect, positive correlation is defined by $\alpha = 1$. For the sake of brevity, the SDF states of Z and X for $\alpha = 1$ are said to be correlated. (If $\alpha = -1$, then the SDF are anti-correlated.) Thus, when the SDF of states Z and X are correlated, Δ_a (see Figure 6) is independent of ω_B within the Z-band and equal to $\bar{\omega}_Z - \bar{\omega}_X$. That is, hole a should track ω_B. We emphasize that because the satellite holes track ω_B to within $\pm$ 1 cm^{-1}, the value of α would have to be very close to 1. Correlation is transitive, i.e., if, for example, the SDF of states Z and X and the SDF of states Y and X are correlated, so are the SDF of states Z and Y. Interpretation B of satellite holes a,b,c rests on the SDF of the three states that contribute to the 825 nm being correlated.

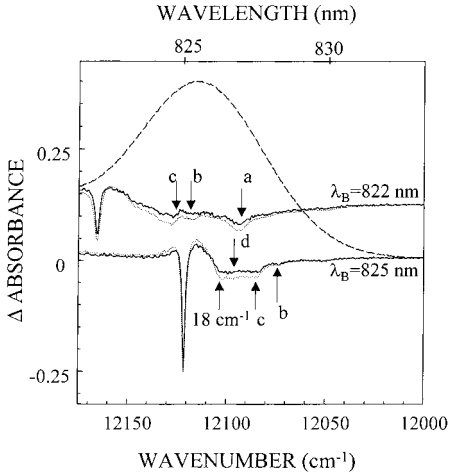

Figure 7. Polarized hole burned spectra of the FMO complex from *P. aestuarii* obtained with burn wavelengths 822.0 and 825.0 nm, $T =$ 4.2 K. Dark solid spectrum: horizontal polarization and dotted spectrum: vertical polarization.

Correlation also means that the SDF of the three states are identical. We note that if the three states are equispaced, only two holes should be observed because $\Delta_b = \Delta_c$, see Figure 6.

Arguments Against Interpretation B. As mentioned, low energy satellite hole structure as rich as that seen in Figure 4 has not been reported for other antenna complexes. Typically, the low-frequency structure is confined to a single pseudo-PSBH at ∼20−30 cm^{-1} with a width of ∼20−30 cm^{-1}.[24,25] (Very recently, a detailed study of the satellite structure associated with the lowest exciton level (B870) of the LH2 BChl *a* complex of *Rb. sphaeroides* revealed only a pseudo-PSBH with an energy of 16 cm^{-1} and a width of 10 cm^{-1}, unpublished results.) Thus, it was that we were led to consider interpretation B which has holes a, b, and c due to correlated EET. Holes e and f would be due to correlated EET from a state located at the low energy side of the intense 815 nm band[6] to the states that contribute to the 825 nm band.

There are several problems with interpretation B. *First*, it is not at all clear why the SDF of the three states (X,Y,Z) that contribute to the 825 nm band should be correlated since they are most likely quite highly localized on the three subunits of the trimer. Furthermore, correlation has not been observed for other photosynthetic complexes, vide infra. The *second problem* arises because, with correlation, one expects that the widths of the satellite holes should equal that of the resonant hole under the following conditions: (i) the homogeneous width of the ZPL of the lower energy state that gives rise to a satellite hole is narrower than that of the ZPL at ω_B; and (ii) spectral diffusion broadening of the satellite holes due to the heat released in downward EET is negligible. The results of ref 11 and those in Figure 9 establish that condition (i) is met, see the Introduction. Broadening due to spectral diffusion of the type defined by (ii) has recently been observed.[26,27] However, it is over 2 orders of magnitude smaller than the widths of the satellite holes in the spectra shown in Figures 4 and 5. The widths of the satellite holes are given in Table 1. We conclude, therefore, that the contribution from spectral diffusion to the widths of the satellite holes is negligible. The widths of the resonant holes of the spectra shown in Figure 4 are given in the caption to that figure. Consider hole a, which is relatively well resolved (Figures 4 and 5). In the $\lambda_B = 824.7-821.0$ nm spectra, its width is significantly broader than that of the resonant hole. This is inconsistent with correlation. Furthermore, the width of hole a in the spectra of Figure 4 is constant to within $\pm$ 2 cm^{-1}. The

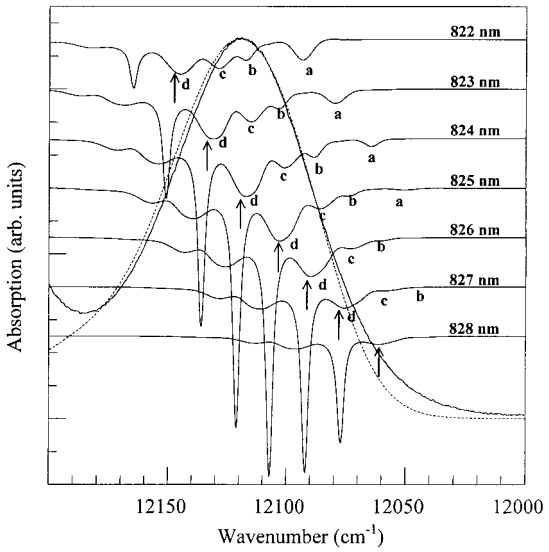

Figure 8. Calculated hole spectra for different burn wavelengths (822−828 nm). The deepest hole in each spectrum is the resonant hole at λ_B. The arrow locates the 18 cm^{-1} pseudo-PSBH. Satellite holes a−d correspond to those shown in Figure 5. The experimental (solid curve) and calculated absorption (dashed curve) spectra are also shown. The values of Huang−Rhys factors (S) and widths of the one-phonon profiles used are given in Table 2; see text for further discussion.

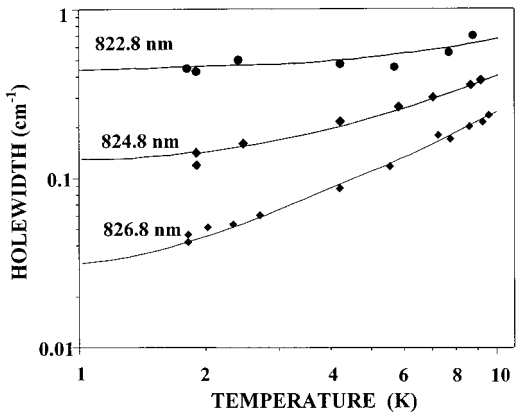

Figure 9. Temperature dependence of zero-phonon holes burned at 822.8, 824.8, and 826.8 nm. The solid curves are fits obtained using eq 3; see text for further discussion.

average of the widths is 10 ± 2 cm^{-1}. For hole a to be a satellite hole due to correlated EET, its width in the top two spectra would have to be significantly broader than in the $\lambda_B = 824.7-822.0$ nm spectra because the width of the resonant hole in the former spectra of 7 cm^{-1} is a factor of 2.5 broader than those in the latter spectra. Clearly, the width of hole a does not reflect the width of the resonant hole. This is inconsistent with correlated EET. The *third problem* is best illustrated using hole a. With correlation and constant burn fluence conditions, its intensity (Δ absorbance (ΔA) value) should be highest when $\omega_B = \bar{\omega}_Z$ (Figure 6). The spectra of Figure 4 lead to a $\bar{\omega}_Z$-value close to 12 180 cm^{-1} (821 nm). The ΔA-values for $\lambda_B = 820$, 821, and 822 nm are 0.024, 0.034, and 0.024, respectively. Correlation also requires that the frequency at which hole a attains its maximum intensity be equal to $\bar{\omega}_X$ which, based on the spectra in Figure 4, corresponds to a wavelength close to 825 nm. The problem is that with the X and Z bands located near 825 and 821 nm and the requirement that the widths of the SDF of the X, Y, and Z states be equal, vide supra, an acceptable fit of the 825 nm absorption band was not achieved, especially on its low energy side (results not shown). Our attempts at fitting were quite intensive and took into account the weak electron−phonon coupling that introduces a slight asymmetry to the X, Y, and Z bands (the SDF were taken to be Gaussians). The position of the Y band associated with hole b was allowed to vary, within reasonable bounds, because the apparent position of hole b ($\Delta_b = 48$ cm^{-1}) may not be its true position because, for example, of interference from the anti-hole a. The intensities of the three bands were independently varied but under the constraint that the intensity of the Z-band must be significantly weaker than those of the other two bands given its location at 821 nm and the experimental 825 nm absorption band, Figure 4.

Putting aside the fitting problem, it is interesting to note that based on the results of excitonic calculations given in refs 8 and 9 one would associate the Z-band with the weakly absorbing A state of the trimer with the main part of the experimental 825 nm band, due to the more strongly allowed E state, which is split into two components (X and Y) because of heterogeneity. The unequal absorption intensities of the three states then means that one is not in the strong energy disorder limit and that polarization effects associated with the 825 nm band should be observable. The polarized triplet−singlet difference spectra reported by van Mourik et al.[7] clearly show that significant polarization effects exist. Their results led us to perform polarized hole burning experiments as described in section 2, the reason being that if holes a, b, and c are due to correlated downward EET, one should observe differences in the values of their $I_{||}/I_{\perp}$ ratio, where $I_{||}$ and $I_{\perp}$ are the intensities of the hole measured with polarization parallel and perpendicular to the burn laser polarization. The results for $\lambda_B = 822$ and 825 nm are shown in Figure 7 where the solid and dotted spectra correspond to $I_{||}$ and $I_{\perp}$, respectively. The resonant holes at λ_B are essentially unpolarized because it was necessary to burn them to saturation depth in order to be able to detect the satellite holes. The two spectra in Figure 7 show that the 18 cm^{-1} pseudo-PSBH and satellite holes a, b, and c are, for all intents and purposes, uniformly and preferentially polarized parallel to the laser polarization. Thus, the results provide no support for holes a, b, and c being due to correlated EET in the weak energy disorder limit. (In the strong disorder limit, the polarizations of the X, Y, and Z states would be identical.) They are, however, consistent with holes a, b, and c also being pseudo-PSBH because the $S_0 \rightarrow Q_y$ electronic transition is strongly allowed, which means that the Condon approximation should be applicable. In the Condon approximation, the phonon sidebands should carry the same polarization as that of the pure electronic transition.

In summary, several reasons for satellite holes a, b, and c not being due to correlated EET have been given. To the best of our knowledge, correlation has not been observed for a photosynthetic complex. In the absence of correlation, a low energy satellite hole that results from EET should mirror the absorption band of the state (acceptor) in which hole burning occurs. The first reported example of an absence of correlation was for the phycobilisomes of a blue-green algae.[28] For this complex, the donor and acceptor states involved in EET are the S_1-states of phycocyanin and allophycocyanin, respectively. Somewhat later, an absence of correlation was reported[29] for the isolated reaction center of photosystem II of green plants where the donor state(s) are associated with Chl *a* molecules and the acceptor state that of the pheophytin *a* molecule active in primary charge separation. Another early example is the LH2 antenna complex of purple bacteria.[30] In that work, it was shown that the SDF of the cyclic ring of B800 BChl *a* donor states are

TABLE 2. Parameter Values Used in Calculations and BChl *a* Vibrational Energies[a]

phonon energy (cm^{-1})[b]	S[c]	width (cm^{-1})[d]	RR modes[e] (cm^{-1})
18	0.24	10	n.o.[f]
72(a)	0.12	7.5	56,72
48(b)	0.04	5.0	56
36(c)	0.12	10	36
24(d)	0.05	5.0	n.o.
120(e)	0.09	10	118
165(f)	0.09	10	163

[a] The 120 and 165 cm^{-1} modes were not included in the calculations. Their *S* values were determined using the value of 0.12 for the 72 cm^{-1} mode and the $\lambda_B = 820$, 819, and 818 nm hole spectra shown in Figure 4 and the spectrum for $\lambda_B = 817$ nm (not shown). [b] The letters in parentheses identify the phonon frequencies with the low energy satellite holes seen in the spectra of Figure 4. [c] *S* = Huang−Rhys factor. [d] Full-width at half-maximum of the one-phonon profile. [e] BChl *a* vibrational energies from resonance Raman experiments on the Q_y-states of the *Rb. sphaeroides* reaction center, from ref 23. [f] Not observed or calculated.

largely uncorrelated with those of the B850 ring of BChl *a* molecules. The reader interested in more recent examples is referred to refs 19, 20, and 31. We note that in the $\lambda_B = 818$ and 819 nm spectra of Figure 4, holes a, e, and f are superimposed on a broad hole. We assign the latter hole to uncorrelated EET from the state(s) excited at λ_B to the states that contribute to the 825 nm band.

Interpretation A of the Satellite Structure. This interpretation has the satellite holes a, b, c, e, and f assigned to pseudo-PSBH with peak energies of 72, 48, 36, 120, and 165 cm^{-1}, respectively. (Thus, with the assignment of the 18 and 24 cm^{-1} satellite hole to pseudo-PSBH, one has a total of seven pseudo-PSBH.) For this assignment to be convincing, it is necessary to show (i) that the dependencies of the hole intensities on λ_B seen in Figure 4 are consistent with the pseudo-PSBH assignment and (ii) that reasonable assignments for the phonons associated with the PSBH exist. Considered first is the question raised by (ii).

The phonons associated with the 18 and 24 cm^{-1} holes are assigned as intermolecular since modes in this energy range are routinely observed in the line-narrowed spectra of π-conjugated chromophores in polymers, glasses and proteins (for a review see ref 25). Such phonons have been assigned to the so-called "boson peak" unique to amorphous solids.[32,33] They are too low in energy to be assigned to intramolecular modes of chlorophyll molecules.[23] However, resonance Raman (RR) spectra of the Q_y-states of BChl *a* molecules in the reaction center of *Rb. sphaeroides* and in BChl *a* films have revealed quite rich structure between 36 and ~160 cm^{-1}. The reader is referred to Czarnecki et al.[23] for the most recent RR data and a review of previous RR data on the Q_y-states of BChl *a*. Semiempirical quantum chemical calculations of the fundamental vibrations of the BChl *a* molecule are also presented. There is a reasonable correlation between the peak energies of holes a, b, c, e, and f and the RR energies which were assigned in [23] to intramolecular modes (Table 2). We say reasonable because the frequencies and relative intensities of the low energy intramolecular modes determined by RR depend, quite significantly, on the Q_y-state being resonantly excited. Furthermore, the RR mode energies are those of the ground state while those determined by hole burning are those of the excited state. The RR bands at energies $\lesssim 130$ cm^{-1} were assigned to vibrations that primarily involve the acetyl and methyl substituents on ring *I*.

Presented next are the results of simulations that determine whether the dependencies of the satellite hole intensities on λ_B seen in Figures 4 and 5 are consistent with their assignment to pseudo-PSBH. Because the satellite hole structure is interfered with by anti-holes and a broad underlying hole due to downward uncorrelated EET, we did not attempt to obtain exact fits; thus, the focus on intensities. The results are shown in Figure 8. Before discussing them, it is appropriate first to briefly discuss the expression of Hayes et al.[22] used in the calculations.

In the low-temperature limit, the expression of Hayes et al. for the absorption spectrum following a burn for time τ reduces to

$$A_\tau(\Omega) = e^{-S_t} \prod_k \sum_{R=0}^{\infty} \left(\frac{S_k^R}{R!}\right) \times \int d\nu\, N_0(\nu - \nu_m) e^{-\sigma P \phi \tau L(\omega_B - \nu)} 1_{R,k}(\Omega - \nu - R\omega_k) \quad (1)$$

This equation does not account for anti-hole absorption. The hole burned spectrum is given by $A_\tau(\Omega) - A_{\tau=0}(\Omega)$. S_k and ω_k are the Huang−Rhys factor and frequency of the *k*th contributing mode; S_t is the total Huang−Rhys factor $\Sigma_k S_k$. The zero-phonon line (ZPL) transition corresponds to $R = 0$. A Lorentzian with a width of 1 cm^{-1} (determined by the instrument resolution) was used for the ZPL. The 1-phonon, 2-phonon, and so forth transitions are defined by $R = 1$, 2, and so forth. The results in Figure 8 were obtained using Gaussian profiles for the 1-phonon transitions of the contributing modes. (Use of Lorentzian or asymmetric profiles yielded results that do not differ significantly.) The widths of the $R \geq 2$ profiles are obtained by folding the 1-phonon profile *R*-times. N_0 $(\nu - \nu_m)$ is the distribution function (SDF) for the ZPL frequencies (ν); ν_m is the peak frequency of the SDF. Because the 825 nm band is contributed to by three states, N_0 was taken to be the sum of three Gaussians, vide infra. In the exponential of eq 1, σ is the integrated absorption cross-section, *P* is the photon flux and ϕ is the hole burning quantum yield. Because values for σ and ϕ are unavailable, $\sigma P\phi$ was an adjustable parameter in the calculations. The single value for $\sigma P\phi$ used was obtained by fitting. Treating $\sigma P\phi$ as a parameter does not affect the λ_B-dependencies of the ΔA-values of the satellite holes. Finally, $L(\omega_B - \nu)$ is given by

$$L(\omega_B - \nu) = e^{-S_t} \prod_k \sum_{R=0}^{\infty} \left(\frac{S_k^R}{R!}\right) 1_{R,k}(\omega_B - \nu - R\omega_k) \quad (2)$$

Here, ω_B is the burn frequency. With ω_B replaced by Ω, $L(\Omega - \nu)$ is the absorption spectrum of a single site with a ZPL frequency equal to ν.

The solid curve in Figure 8 is the experimental 825 nm absorption band. The dashed curve is the 825 nm band calculated using eq 1 with $\tau = 0$. The SDF of the three contributing states were taken to carry equal intensities and widths (50 cm^{-1}) and to be equispaced (20 cm^{-1}). (Allowance for unequal intensities and spacings, subject to the constraint of a reasonable fit to the 825 nm band, resulted in hole spectra that mimic the intensity behavior of the satellite holes seen in the spectra of Figure 8). Because the S-factors of the contributing modes are small, Table 2, the asymmetry that they introduce to the calculated 825 nm band is small. Except for the low energy tail, the agreement between the calculated and experimental profiles of the 825 nm band is quite reasonable. The sharpest and deepest hole in the calculated spectra is the resonant hole coincident with the burn wavelength. The Huang−Rhys factors of the contributing modes and the widths of their one-phonon profiles used are given in

Table 2. The hole spectra were calculated at intervals of 1 nm across the absorption band. Therefore, the resonant hole positions are akin to those of Figures 4 and 5. The fractional absorbance changes of the resonant holes are, from top to bottom, 0.31, 0.46, 0.56, 0.62, 0.68, 0.74, and 0.81. These values mimic the trend set by the experimental values given in the caption to Figure 4. The explanation for this trend is that as the burn frequency is tuned to the blue, the probability of exciting phonon transitions increases while the probability of exciting ZPL transitions decreases. This leads to a decrease and increase in the intensity of the resonant hole and pseudo-PSBH, respectively.[34,35] This intensity behavior is evident in the experimental spectra shown in Figures 4 and 5 and calculated spectra in Figure 8. Moreover, one observes that the intensities of the satellite holes reach their maximum values when they are located near the maximum of the 825 nm band. The agreement between the observed and calculated spectra is better than qualitative. To illustrate this, we consider the 18 cm^{-1} pseudo-PSBH indicated by the solid arrows in Figures 4, 5, and 8. When combined, the results of Figures 4 and 5 lead to relative intensity (ΔA) values for $\lambda_B = 828$, 827, 826, 825, 824, and 823 nm of 0.2, 0.5, 0.7, 0.9, 1.0, and 0.7, respectively. The corresponding values from Figure 8 are 0.13, 0.36, 0.68, 0.92, 1.0, and 0.85. We consider the agreement satisfactory given that there is considerable uncertainty in the experimental ΔA values. It should be noted that real-PSBH that lie to higher energy of the resonant hole also appear in the calculated spectra. In the experimental spectra, they are interfered with by the antihole.

The Huang−Rhys factors and widths of the one-phonon profiles given in Table 2 can be used in the calculation of EET rates involving the states that contribute to the 825 nm band.

Energy Transfer and Spectral Dynamics of the Three Lowest Energy States. Figure 9 shows the temperature dependencies of the widths (fwhm) of ZPH burned at 822.8, 824.8, and 826.8 nm. They are very similar to those shown in Figure 3 of ref 11 for *Cb. tepidum*, where burn wavelengths of 823.0, 825.0, and 827.0 nm were used. (The 0.2 nm shift between the burn wavelengths is a consequence of the absorption maximum of the 825 nm band of *P. aestuarii* being at a wavelength 0.2 nm longer than that of *Cb. tepidum*.) The discussion that follows is similar to that given in ref 11.

That the temperature dependence of the 822.8 and 824.8 nm holewidths are considerably weaker than that of the 826.8 nm holewidth, especially below ~4 K, suggests that the widths of the former two holes at 1.8 K are dominated by a temperature-independent contribution, one that is attributed to downward energy transfer. Preliminary analysis of the 826.8 nm data points showed that they approximately follow a T^{α} dependence with $\alpha \approx 1.3$. This power law is unique to pure dephasing/spectral diffusion due to two-level systems (TLS) of glasses and proteins. Such a temperature dependence has recently been reported for the lowest energy Q_y-state of the photosystem II reaction center,[36] the LHC II antenna complex of photosystem II,[19] and the lowest exciton level of the B850 molecules in the LH2 antenna complex of purple bacteria.[37] However, the hole widths for $\lambda_B = 826.8$ nm are not solely determined by the TLS. This follows because of the apparent convergence of the holewidths for the three burn wavelengths at higher temperatures. That is, if the 826.8 nm holewidths were due only to TLS, they should add to the energy transfer contributions to the widths of the 822.8 and 824.8 nm holes. The EET kinetics can be safely assumed to be temperature independent for $T \leq 10$ K. This line of argument becomes more convincing when the holewidths in Figure 9 are fit by

$$\Gamma_{hole}(cm^{-1}) = \Gamma_0 + 2AT^{\alpha} \quad (3)$$

where Γ_0 is temperature independent and the second term is due to TLS-induced spectral dynamics. The 826.8 nm data were fit first (solid curve), resulting in $\Gamma_0 = 0.015$ cm^{-1}, $\alpha = 1.3$, and $A = 0.0056$ (Table 3). The lifetime of the lowest energy state is 2 ns.[10,11] The lifetime contribution to Γ_0 is given by $2(2\pi T_1 c)^{-1}$, where T_1 is the lifetime and c is the speed of light in the units of cm · s^{-1}. The lifetime contribution is 0.005 cm^{-1}, leaving ~0.010 cm^{-1} of Γ_0 to be explained. As in ref 11, we attribute the 0.010 cm^{-1} to spectral diffusion and/or a small contribution to the holewidth from the next higher energy state near 824.8 nm. For fitting of the 824.8 and 822.8 nm data, α was fixed at 1.3, leaving Γ_0 and A as the only adjustable parameters. That $A = 0.0056$ for the three λ_B-values, Table 3, supports our analysis procedure because the spectral dynamics from TLS should be the same for the three subunits of the trimer. As in refs 9 and 10 the Γ_0-values obtained for $\lambda_B = 824.8$ and 822.8 nm are assigned to lifetime broadening due to downward EET. They lead to the T_1 values of 99 and 26 ps given in Table 3.

TABLE 3. Analysis of Zero-Phonon Holewidths of the Three States that Contribute to the 825 nm Band

λ_B(nm)	T_1(ps)[a]	A($cm^{-1}K^{-a}$)[b]	α[b]
	P. aestuarii		
822.8	26	.0056	1.3
824.8	99	.0056	1.3
826.8	2×10^3 [c]	.0056	1.3
	Cb. tepidum (from ref 11)		
823.0	32	0.0070	1.3
825.0	135	0.0070	1.3
827.0	2×10^3	0.0070	1.3

[a] Lifetimes of three contributing states. [b] Parameters associated with pure dephasing/spectral diffusion due to two-level systems, see eq 3. [c] From refs 10 and 11.

For comparison, the values of T_1, A, and α for *Cb. tepidum* are also given in Table 3. That they are similar to those for *P. aestuarii* is not surprising given that the structures of the two species are very similar as are their 825 nm absorption bands, Figure 1. The differences in the above values may not be significant because the λ_B-values used for *P. aestuarii* may not be exactly equivalent to those used for *Cb. tepidum* (keeping in mind that the 825 nm band is due to three overlapping and inhomogeneously broadened bands).

With reference to Figure 6, the T_1 values of *P. aestuarii* for $\lambda_B = 822.8$ and 824.8 nm (823.0 and 825.0 nm for *Cb. tepidum*) are assigned to downward EET from the Z and Y states, respectively. For the latter state, there is only the Y→X pathway whereas for the former, there are the Z→Y and Z→X pathways. At this point, it seems most likely that these EET pathways should be describable in terms of weak coupling nonadiabatic transfer theory. The electron−phonon coupling parameters that define the spectral densities in the rate expression are given in Table 2. It will be interesting to see whether they can explain why the transfer rate for the Z state is four times higher than that of the Y state. Such calculations, which take into account the effects of structural heterogeneity, are now in progress.

4. Conclusions

The nonphotochemical hole burning spectra and spectral dynamics data reported for the FMO complex of *P. aestuarii*

pertain mainly to the lowest energy absorption band at 825 nm, which is contributed to by three states. These states stem from the lowest energy state of the subunit of the trimer. The splittings between them, which can be no greater than about 30 cm^{-1}, appear to be dominated by structural heterogeneity. Earlier hole burning studies had shown that the widths of the three underlying absorption bands are mainly inhomogeneously broadened ($\sim$50 cm^{-1}) at liquid helium temperatures. The two main objectives of our experiments were to interpret the rich low energy satellite hole structure observed when the burn wavelength (λ_B) is located in the 825 nm band and to determine the excitation energy transfer (EET) kinetics for the two higher energy states that contribute to the 825 nm band.

The λ_B-dependent hole spectra obtained are the most detailed yet reported for an antenna complex. They reveal low energy satellite holes at 18, 24, 36, 48, and 72 cm^{-1}, as measured relative to the resonant zero-phonon hole at λ_B. The last four holes are designated as holes d, c, b, and a, respectively, in Table 1 which also includes the energies of two higher energy satellite holes. The 18 and 24 cm^{-1} holes are assigned to pseudo-phonon sideband hole (PSBH) due to intermolecular phonons. Two interpretations for holes c, b, and a at 36, 48, and 72 cm^{-1}, respectively, were considered. The interpretation that has them due to correlated EET from the two higher energy states that contribute to 825 nm band could be rejected. Thus, the FMO complex is yet another example where the site distribution functions of different states exhibit little correlation. On the basis of theoretical simulations of the λ_B-dependence of the hole spectra, we conclude that the above holes are pseudo-PSBH and that the 36, 48, 72, 120, and 165 cm^{-1} phonons are most likely due to BChl *a* intramolecular modes. Their Huang−Rhys factors and one-phonon profile widths are given in Table 2.

The temperature dependencies (1.8−10 K) of the widths of zero-phonon holes burned in the 825 nm band of *P. aestuarii* at λ_B = 822.8, 824.8, and 826.8 nm were found to be similar to those of *Cb. tepidum*, Table 3. These wavelengths should be close to the absorption maxima of the three states that contribute to the 825 nm band, Z, Y, and X in Figure 2. Pure dephasing/spectral diffusion due to the glasslike two-level systems of the protein is operative and identical for the three states. When this contribution to the holewidths is taken into account the time constants for excitation energy transfer from the Y to X state and Z to Y and X states are 99 and 26 ps, respectively. Currently, energy transfer calculations are in progress that utilize the electron−phonon coupling parameters given in Table 2 with due account being given to the effects of energy disorder.

Acknowledgment. Research at the Ames Laboratory was supported by the Division of Chemical Sciences, Office of Basic Energy Sciences, U.S. Department of Energy. Ames Laboratory is operated for USDOE by Iowa State University under Contract W-7405-Eng-82. We are indebted to Professor T. Aartsma of Leiden University for providing the samples of the FMO complex from *P. aestuarii*.

References and Notes

(1) Fenna, R. E.; Matthews, B. W.; Olson, J. M.; Shaw, E. K. *J. Mol. Biol.* **1974**, *84*, 231.

(2) Blankenship, R. E.; Olson, J. M.; Miller, M. In *Anoxygenic Photosynthetic Bacteria*; Blankenship, R. E., Madigan, M. T., Bauer, C. E., Eds.; Kluwer: Dordrecht, 1995; pp 399−435.

(3) Savikhin, S.; Buck, D. R.; Struve, W. S. *J. Phys. Chem. B* **1998**, *102*, 5556.

(4) Lu, X.; Pearlstein, R. M. *Photochem. Photobiol.* **1993**, *57*, 86.

(5) Li, Y. F.; Zhou, W.; Blankenship, R. E.; Allen, J. P. *J. Mol. Biol.* **1997**, *271*, 456.

(6) Johnson, S. G.; Small, G. J. *J. Phys. Chem.* **1991**, *95*, 471.

(7) van Mourik, F.; Verwijst, R. R.; Mulder, J. M.; van Grodelle, R. *J. Phys. Chem.* **1994**, *98*, 10 307.

(8) Gülen, D. *J. Phys. Chem.* **1996**, *100*, 17 684.

(9) Louwe, R. J. W.; Vrieze, T.; Aartsma, T. J.; Hoff, A. J. *J. Phys. Chem. B* **1997**, *101*, 11 280.

(10) Louwe, R. J. W.; Aartsma, T. J. *J. Phys. Chem.* **1997**, *101*, 7221.

(11) Rätsep, M.; Blankenship, R. E.; Small, G. J. *J. Phys. Chem. B* **2000**, *103*, 5736.

(12) Franken, E. M.; Neerken, S.; Louwe, R. J. W.; Amesz, J.; Aartsma, T. J. *Biochemistry* **1998**, *37*, 5046.

(13) Holt, S. C.; Conti, S. F.; Fuller, R. C. *J. Bacteriol.* **1996**, *91*, 311.

(14) Francke, C.; Amesz, J. *Photosyn. Res.* **1997**, *53*, 137.

(15) Shu, L.; Small, G. J. *J. Opt. Soc. Am.* **1992**, *9*, 733, and references therein.

(16) Shu, L.; Small, G. J. *J. Opt. Soc. Am.* **1992**, *9*, 724.

(17) Kim, W.-H.; Reinot, T.; Hayes, J. M.; Small, G. J. *J. Phys. Chem.* **1995**, *99*, 7300.

(18) Reddy, N. R. S.; Kolaczkowski, S. V.; Small, G. J. *J. Phys. Chem.* **1993**, *97*, 6934.

(19) Pieper, J.; Rätsep, M.; Jankowiak, R.; Irrgang, K.-D.; Voigt, J.; Renger, G.; Small, G. J. *J. Phys. Chem. A* **1999**, *103*, 2412.

(20) Pieper, J.; Irrgang, K.-D.; Rätsep, M.; Voigt, J.; Renger, G.; Small, G. J. *Photochem. Photobiol.* **2000**, in press.

(21) Milanovich, N.; Hayes, J. M.; Small, G. J. *Mol. Cryst. Liq. Cryst.* **1996**, *291*, 147.

(22) Hayes, J. M.; Lyle, P. A.; Small, G. J. *J. Phys. Chem.* **1994**, *98*, 7337.

(23) Czarnecki, K.; Diers, J. R.; Chynwat, V.; Erickson, J. P.; Frank, H. A.; Bocian, D. F. *J. Am. Chem. Soc.* **1997**, *119*, 415, and references therein.

(24) Jankowiak, R.; Small, G. J. In *Photosynthetic Reaction Centers*, Deisenhofer, J. and Norris, J., Eds.; Academic Press: New York, 1993; p 133.

(25) Small, G. J. *Chem. Phys.* **1995**, *197*, 239.

(26) den Hartog, F. T. H.; Bakker, M. P.; Silbey, R. J.; Völker, S. *Chem. Phys. Lett.* **1998**, *297*, 314.

(27) den Hartog, F. T. H.; van Papendrecht, C.; Silbey, R. J.; Völker, S. *J. Chem. Phys.* **1999**, *110*, 1010.

(28) Köhler, W.; Friedrich, J.; Fischer, R.; Scheer, H. *J. Chem. Phys.* **1988**, *89*, 871.

(29) Tang, D.; Jankowiak, R.; Seibert, M.; Yocum, C. F.; Small, G. J. *J. Phys. Chem.* **1990**, *94*, 6519.

(30) Reddy, N. R. S.; Small, G. J.; Seibert, M.; Picorel, R. *Chem. Phys. Lett.* **1991**, *181*, 391.

(31) Rätsep, M.; Johnson, T. W.; Chitnis, P. R.; Small, G. J. *J. Phys. Chem. B* **1999**, *104*, 836.

(32) Ahn, J. S.; Kanematsu, Y.; Kushida, T. *Phys. Rev. B* **1993**, *48*, 9058.

(33) Kanematsu, Y.; Ahn, J. S.; Kushida, T. *Phys. Rev. B* **1993**, *48*, 9066.

(34) Lee, I. J.; Hayes, J. M.; Small, G. J. *J. Chem. Phys.* **1989**, *91*, 3413.

(35) Lyle, P. A.; Kolaczkowski, S. V.; Small, G. J. *J. Phys. Chem.* **1993**, *97*, 6926 and references therein.

(36) den Hartog, E. T. H.; Vacha, F.; Lock, A. J.; Barber, J.; Dekker: J. P.; Völker, S. *J. Phys. Chem. B* **1998**, *102*, 9174.

(37) Wu, H.-M.; Rätsep, M.; Lee, I.-J.; Cogdell, R. J.; Small, G. J. *J. Phys. Chem. B* **1997**, *101*, 7654.